Supplementary Material

Correspondence to: Juliette Grosset (juliette.grosset@umontpellier.fr)

1 Filtered GNSS strain rates

GNSS velocities from (Masson et al., 2019) are filtered spatially to derive velocity and horizontal strain rate fields on a regular grid (0.5 x 0.5 degrees) using the method described in (Masson et al., 2019; Mazzotti et al., 2011). At each grid point g, weighted average velocity vector V_g and strain rate tensor $\dot{\varepsilon}_g$ are computed by applying a Gaussian weighting function G_n to the GNSS velocities V_n (also weighted according to standard errors σ_n):

$$V_{gi} = \frac{\left(\sum_{n=1}^{N} \frac{G_n}{\sigma_{ni}^2} V_{ni}\right)}{W_i} \tag{1}$$

$$\dot{\varepsilon}_{gij} = \frac{\log(2)}{r_g^2}\left[\left[\frac{\left(\sum_{n=1}^{N} -\Delta_{nj}\frac{G_n}{\sigma_{ni}^2}V_{ni}\right)}{W_i} - \left(\sum_{n=1}^{N} -\Delta_{nj}\frac{G_n}{\sigma_{ni}^2}\right)\frac{V_{gj}}{W_j}\right] + \left[\frac{\left(\sum_{n=1}^{N} -\Delta_{ni}\frac{G_n}{\sigma_{nj}^2}V_{nj}\right)}{W_j} - \left(\sum_{n=1}^{N} -\Delta_{ni}\frac{G_n}{\sigma_{nj}^2}\right)\frac{V_{gi}}{W_i}\right]\right] \tag{2}$$

$$G_n = e^{-\log(2)\frac{\Delta_n^2}{r_g^2}} \tag{3}$$

$$W_i = \sum_{n=1}^{N} \frac{G_n}{\sigma_{ni}^2} \tag{4}$$

where N is the total number of GNSS velocities, i and j are velocity components (North, East, or Up), r_g is the Gaussian filtering half-width, and Δn is the distance between the computation grid point and the GNSS velocity site n. The impact of

the choice of Gaussian half-width r_g on the filtered GNSS strain rate field is shown in Figures S1.

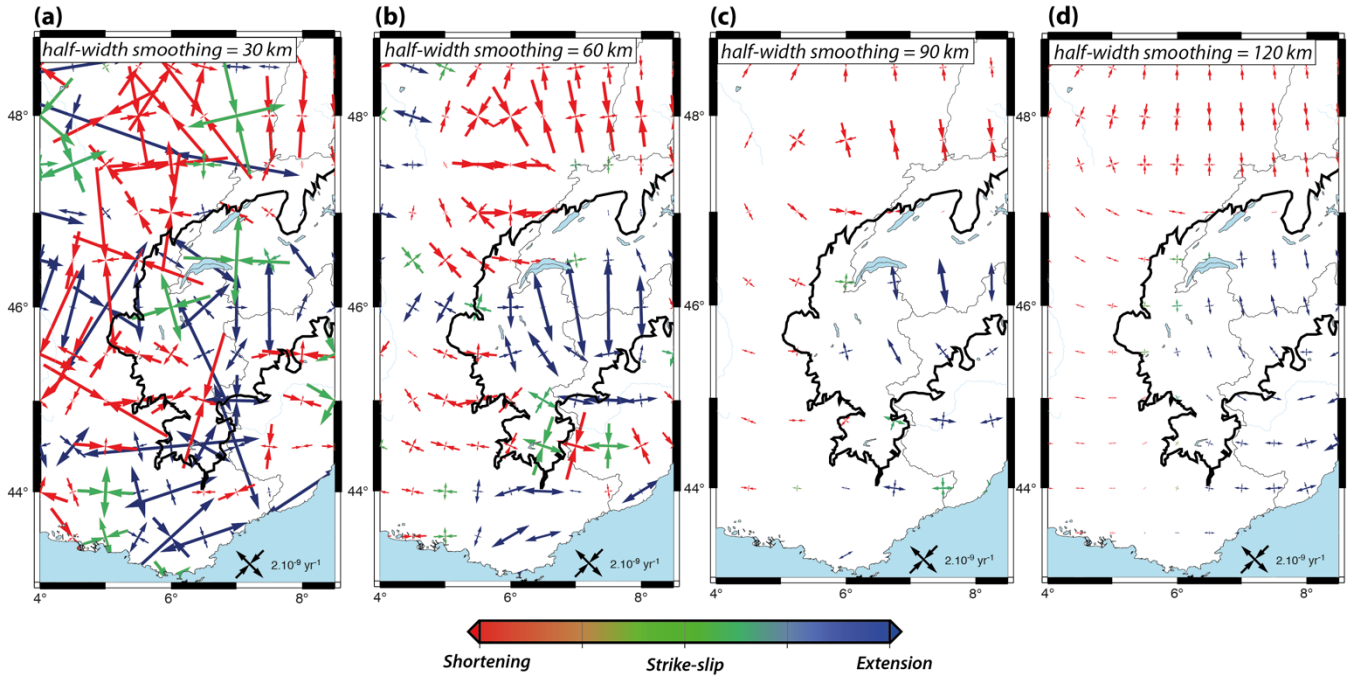

Figure S1 Filtered GNSS Strain rate fields computed for four different Gaussian half-widths. (a) r_g = 30 km, (b) r_g = 60 km, (c) r_g = 90 km, and (d) r_g =120 km. Strain rate tensors are color-coded by deformation style. Black line is Last Glacial Maximum icecap extension (Mey et al., 2016).

2 GIA model comparisons

In order to test the impact of our GIA model simplifications (thin elastic plate over a Newtonian viscous fluid, instantaneous deglaciation), we compare our model predictions with those of a standard "1D Maxwell" model (1D layering, Maxwell visco-elastic rheology) using a 2D finite-element approach (code Adeli, (Chéry and Hassani, 2005)). The "1D Maxwell" model parameterization is based on that of (Steffen et al., 2014) and slightly adapted to be more representative of the Alpine GIA (Fig. S2): elastic plate thickness of 30 km, mantle Maxwell-body layering, 200 km-large / 250 m-thick icecap that builds up over 2 kyr, remains in place for 100 kyr, and melts over 2 kyr. For comparison, the thin elastic plate models use the same ice load and a combination of a plate thickness he = 30 km and a viscous relaxation time τ = 10,000yr, or a plate thickness he = 45 km and a viscous relaxation time τ = 13,000 yr. These plate thicknesses and relaxation times are adapted to the "1D Maxwell" structure of (Steffen et al., 2014) for the purpose of the test (and are thus larger than the best-fit values for the Alpine system based on GNSS data (h_e = 10–20 km, τ = 4500–5500 yr, cf. section 3 of the main text).

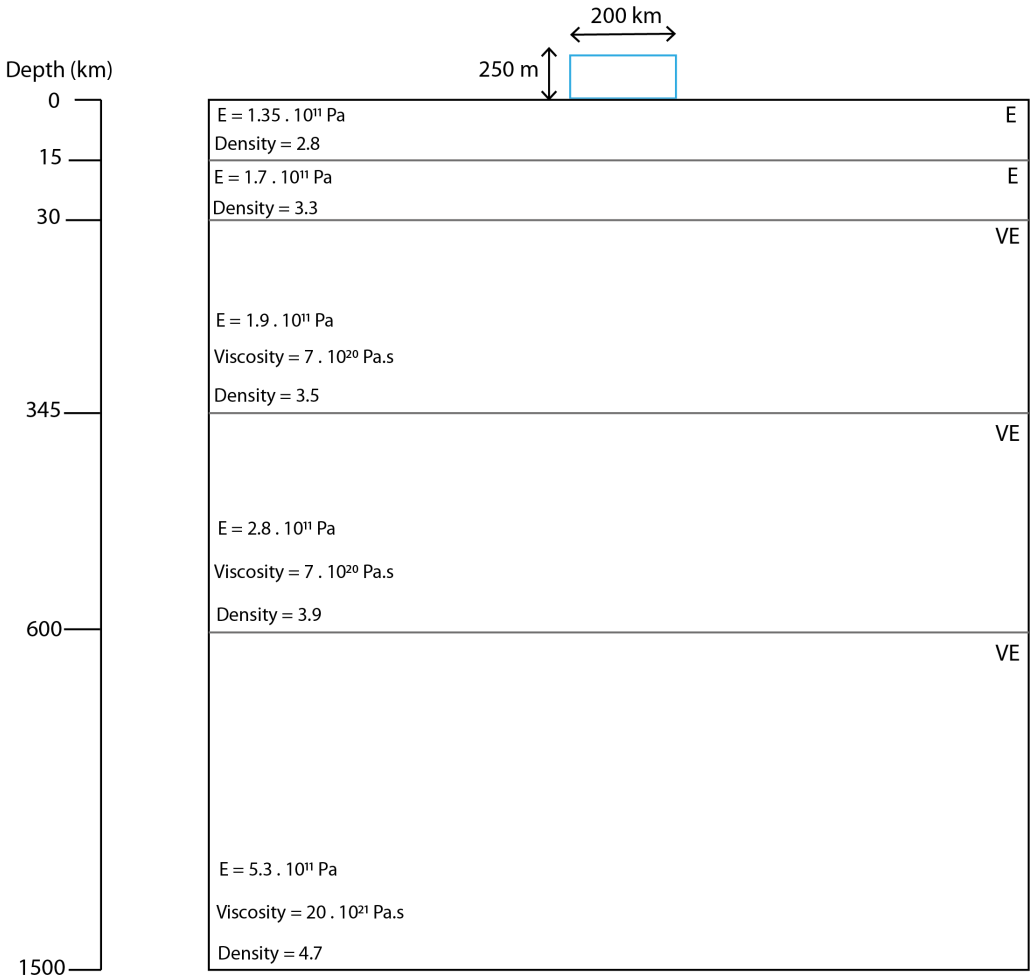

Figure S2 Finite element "1D Maxwell" GIA model setup. Mantle layers (30–1500 km depth) follow a Maxwell-body rheology. Model boundary conditions: Base = hydrostatic restoration; vertical sides = no horizontal slip, no vertical slip; surface = free slip.

Surface predictions (displacement and horizontal stress) of the two types of models are compared in Figure S3 at the glacial maximum and 20 kyr after. Both model types predict a typical flexural response at their surface: subsidence and compression below the ice load, uplift and tension in the lateral forebulges. The "1D Maxwell" model deviates from the analytical thin-plate solution, with an overall tighter flexural shape associated with smaller displacement and stress amplitudes. For the same elastic plate thickness (30 km), the differences between the "1D Maxwell" and "thin-plate" model predictions are ca. 0–10 m in flexure and 0 and ca. 0–3 MPa in horizontal stress. In relative terms, these differences can reach up to 100% of the prediction amplitudes (i.e., factor of 2).

As expected for a multi-layer Maxwell-body model, the surface flexural response of the "1D Maxwell" model shows an equivalent flexural wavelength that changes with time (cf. forebulge extension stress ca. 170 km at glacial maximum vs. 210

km after 20 kyr, Fig. S3). This variation remains very small (a few 10s km) in our test due to the relatively small size of the Alpine icecap and its negligible impact on the deep mantle layers.

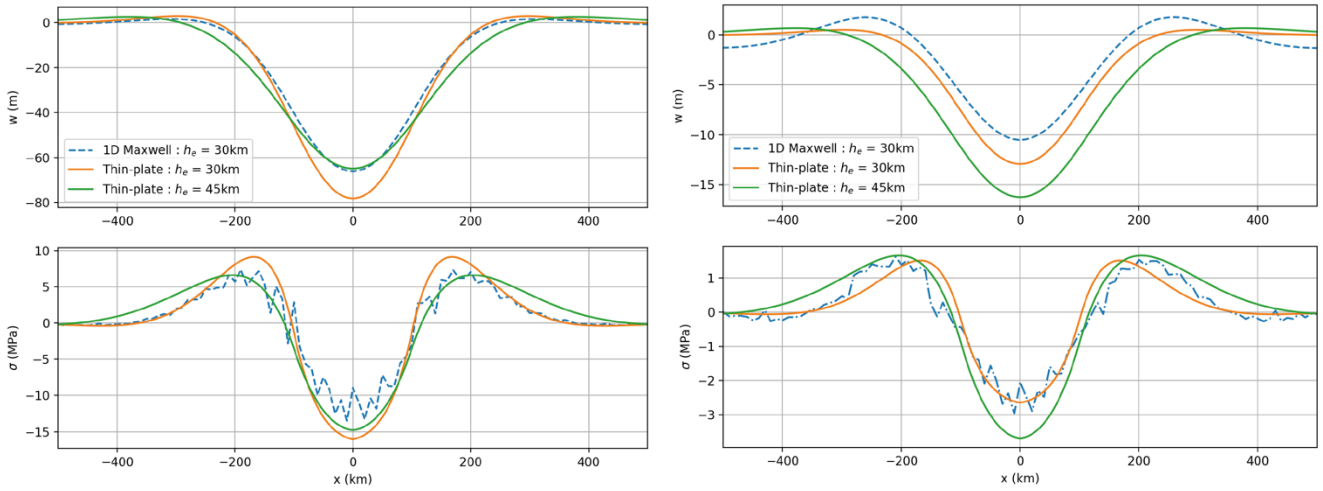

Figure S3. "1D Maxwell" vs. "thin-plate" model predictions. Top row: surface flexure (vertical displacement). Bottom layer: surface horizontal stress. Left column: at glacial maximum. Right column: 20 kyr after glacial maximum.

In Figure S4, we compare the temporal evolution of the surface flexure and stress at the center of the model (center of the ice load). The thin-plate model only represents the post deglaciation phase (assumed to occur instantaneously at the glacial maximum in this case). As mentioned above, at the glacial maximum (110 kyr) the "1D Maxwell" model predictions are ca. 15–20% smaller than those of the "thin-plate" model (for the same elastic thickness of 30 km). This results from the damping effect of the viscous mantle (which is not considered in the "thin-plate" model), even though the mantle is almost fully relaxed following the 100 kyr of ice loading (Fig. S4). These differences vary in sign and amplitude after the deglaciation but remain within less than 10 m and 2 MPa. If we consider the situation 20 kyr after the glacial maximum (i.e., roughly present-day for the Western Alps LGM, cf. text), the "1D Maxwell" and "thin-plate" model predictions are similar in flexure (within a few meters), in vertical uplift rates (0.8 vs. 1.3 mm/yr), and in horizontal stress (within 1 MPa).

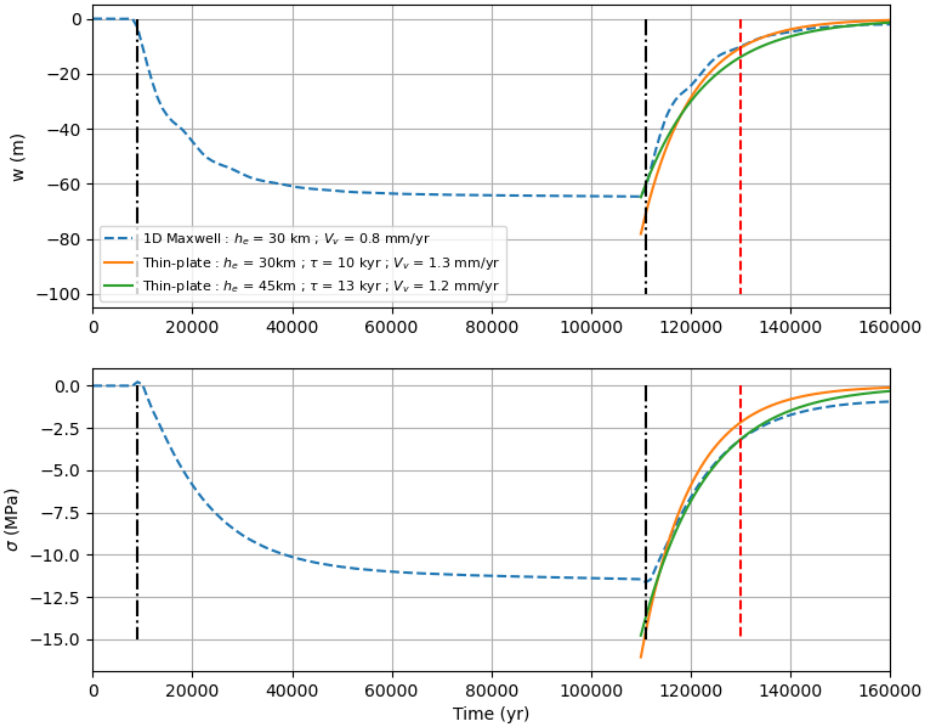

Figure S4. Temporal evolution of "1D Maxwell" vs. "thin-plate" model predictions at the center of the ice load. Top: surface flexure (vertical displacement). Bottom: surface horizontal stress. Vertical black dashed lines indicate the onset and termination of the ice load. The vertical read dashed line indicates 20 kyr post glacial maximum. Glaciation and deglaciation last 2 kyr in the "1D Maxwell" model and are instantaneous in the "thin-plate" model.

Overall, these tests illustrate the similarities in the response of a simple "thin-plate" model with that of a more detailed "1D Maxwell" model in the case of a small icecap load, with differences limited to a few m in flexure and a few MPa in horizontal stress, reaching a factor of two in amplitude in the most extreme cases.

3 GIA strain rates and stresses

Figures S5 and S6 illustrate the GIA present-day horizontal strain rate and stress fields for different model parameterizations.

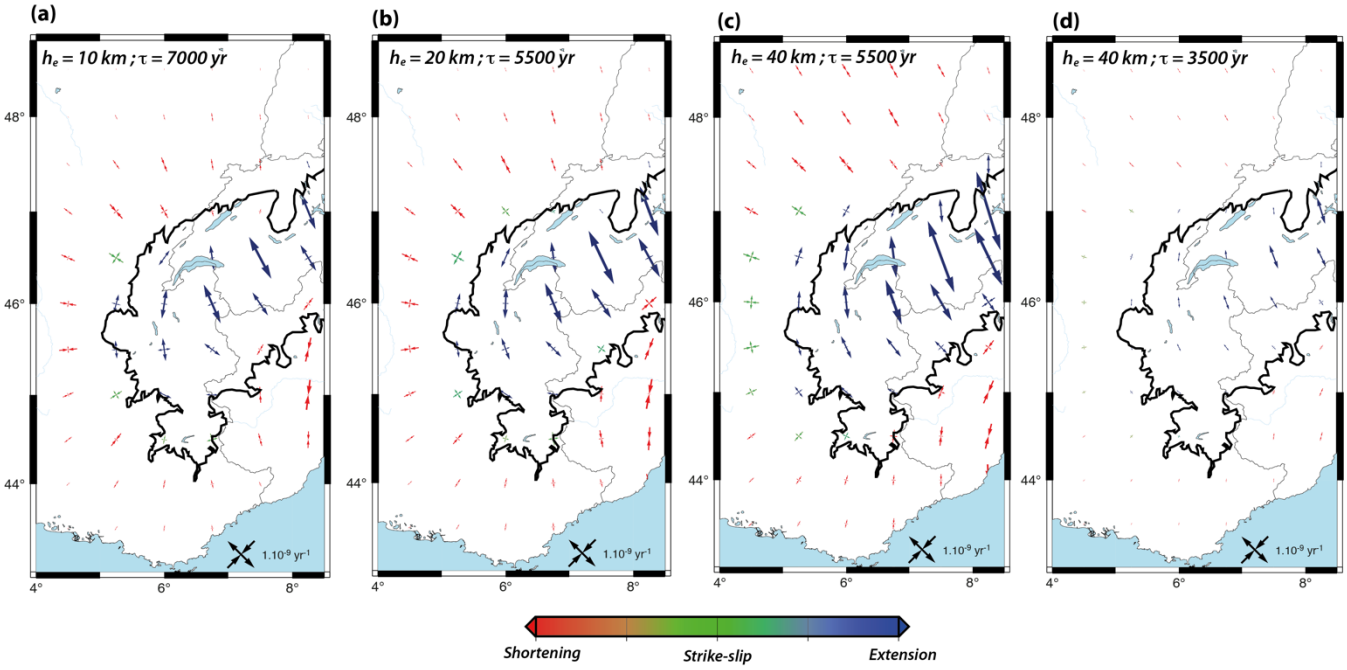

Figure S5. Filtered GIA present-day strain rate fields computed for four model parameter sets. Predictions for GIA model (a) h_e = 10 km, τ = 7000 yr, (b) h_e = 20 km, τ = 5500 yr, (c h_e = 40 km, τ = 5500 yr, and (d) h_e = 40 km, τ = 3500 yr. Strain rate tensors are color-coded by deformation style. Black line is Last Glacial Maximum ice extension (Mey et al., 2016).

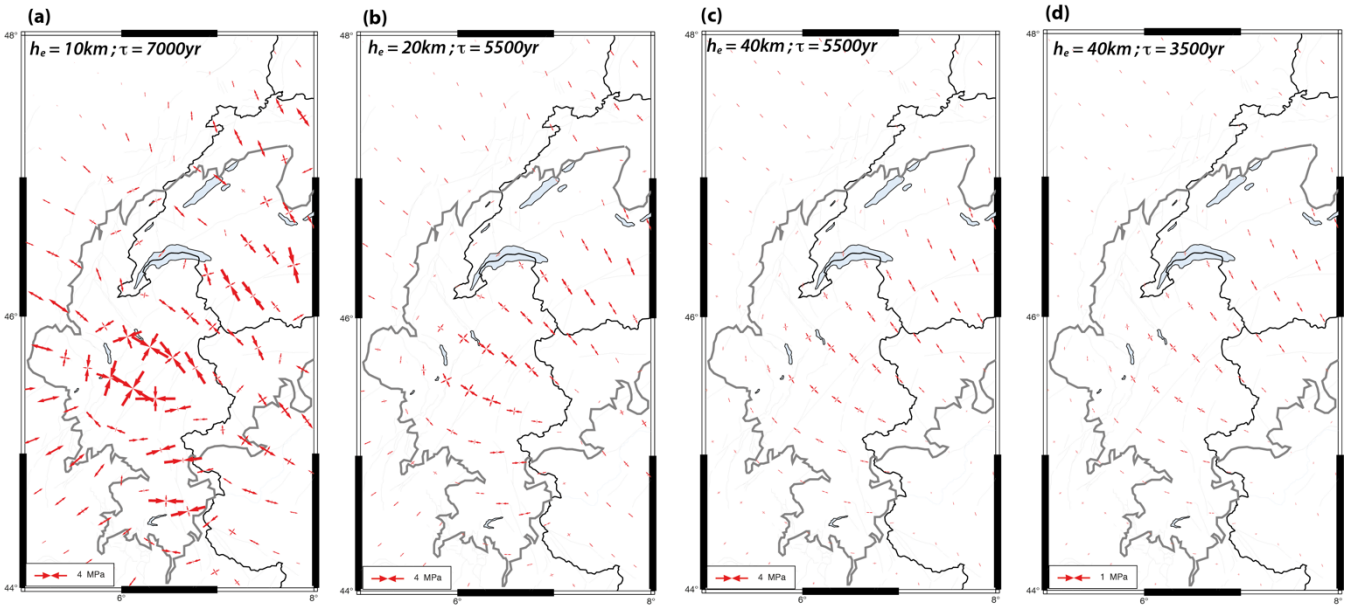

Figure S6. Filtered GIA present-day stress fields computed for four model parameter sets. Predictions for GIA model (a) h_e = 10 km, τ = 7000 yr, (b) h_e = 20 km, τ = 5500 yr, (c h_e = 40 km, τ = 5500 yr, and (d) h_e = 40 km, τ = 3500 yr. Black line is Last Glacial Maximum ice extension (Mey et al., 2016).

References

Chéry, J. and Hassani, R.: ADELI: A 2d/3d finite element software for thermo-mechanical modeling of geological deformation, 2005.

Masson, C., Mazzotti, S., Vernant, P., and Doerflinger, E.: Extracting small deformation beyond individual station precision from dense GNSS networks in France and Western Europe, Solid Earth, 10, 1905–1920, https://doi.org/10.5194/se-10-1905-2019, 2019.

Mazzotti, S., Leonard, L. J., Cassidy, J. F., Rogers, G. C., and Halchuk, S.: Seismic hazard in western Canada from GPS strain rates versus earthquake catalog, J. Geophys. Res., 116, B12310, https://doi.org/10.1029/2011JB008213, 2011.

Mey, J., Scherler, D., Wickert, A. D., Egholm, D. L., Tesauro, M., Schildgen, T. F., and Strecker, M. R.: Glacial isostatic uplift of the European Alps, Nature Communications, 7, 1–9, https://doi.org/10.1038/ncomms13382, 2016.

Steffen, R., Steffen, H., Wu, P., and Eaton, D. W.: Stress and fault parameters affecting fault slip magnitude and activation time during a glacial cycle, Tectonics, 33, 1461–1476, https://doi.org/10.1002/2013TC003450, 2014.